RSC Advances

PAPER

View Article Online
View Journal | View Issue

Check for updates

Cite this: *RSC Adv.*, 2020, **10**, 12891

# Synthesis of plasmonic Fe/Al nanoparticles in ionic liquids†

Alexa Schmitz,[a] Hajo Meyer,[b] Michael Meischein,[b] Alba Garzón Manjón,[c] Laura Schmolke,[a] Beatriz Giesen,[a] Carsten Schlüsener,[a] Paul Simon,[d] Yuri Grin,[d] Roland A. Fischer,[e] Christina Scheu,[c] Alfred Ludwig[b] and Christoph Janiak*[a]

Received 5th February 2020
Accepted 19th March 2020

DOI: 10.1039/d0ra01111h

rsc.li/rsc-advances

Bottom-up and top-down approaches are described for the challenging synthesis of Fe/Al nanoparticles (NPs) in ionic liquids (ILs) under mild conditions. The crystalline phase and morphology of the metal nanoparticles synthesized in three different ionic liquids were identified by powder X-ray diffractometry (PXRD), X-ray photoelectron spectroscopy (XPS), transmission electron microscopy (TEM), selected-area electron diffraction (SAED) and fast Fourier transform (FFT) of high-resolution TEM images. Characterization was completed by scanning electron microscopy with energy dispersive X-ray spectroscopy (SEM-EDX) for the analysis of the element composition of the whole sample consisting of the NPs and the amorphous background. The bottom-up approaches resulted in crystalline FeAl NPs on an amorphous background. The top-down approach revealed small NPs and could be identified as $Fe_4Al_{13}$ NPs which in the IL [OPy][$NTf_2$] yield two absorption bands in the green-blue to green spectral region at 475 and 520 nm which give rise to a complementary red color, akin to appropriate Au NPs.

Open Access Article. Published on 31 March 2020. Downloaded on 2/6/2026 9:28:58 AM.
This article is licensed under a Creative Commons Attribution-NonCommercial 3.0 Unported Licence.

## Introduction

Bimetallic or alloyed nanoparticles (NPs) have attracted increasing interest for a wide range of applications,[1–8] especially showing tuneable properties in terms of their catalytic behaviour.[9] However, most of the studied bimetallic NPs are based on the combination of noble or coinage metals and non-noble transition metals (*e.g.* Pd/Ga,[10] Cu/Fe,[11] Pt/Fe,[12] Ni/Fe,[13] Pd/Fe[12]). The main disadvantage of these combinations is the high costs associated with the use of the noble metals, leading to a strong scientific and industrial desire towards non-noble metal-based catalysts. Accordingly, Cokoja *et al.* described the synthesis of non-noble bimetallic NPs, *e.g.* CoAl,[14] NiAl,[15] $CuAl_x$ ($x = 1, 2$)[16] and $CuE_2$ (E = Al, Ga)[17] by the soft wet-chemical hydrogenolysis of organometallic precursors. Schütte *et al.* reported the synthesis of Ni/Ga[18] and Cu/Zn[19] NPs which were shown to be active catalysts for the semihydrogenation of alkynes and methanol formation, respectively. Recently, Schmolke *et al.* also showed the application of intermetallic Co/Al NPs in alkyne hydrogenation.[20] With regard to potentially low-cost nano catalysts, iron aluminide NPs represent a particularly desirable option given that Fe and Al are both cheap and ubiquitous metals. Furthermore, Armbrüster *et al.* have already shown that bulk $Fe_4Al_{13}$ presents a possible low-cost alternative for Pd in the heterogenous semihydrogenation of acetylene, referring to high conversion and a very high ethylene-selectivity, which was only 6% lower than that of an industrial benchmark catalyst.[21]

Furthermore, bulk FeAl and $Fe_3Al$ alloys are well known for their good corrosion, sulfidation, carburization resistance,[22,23] making them a sought-after material for aggressive and corrosive environments.[24] The corrosion resistance is caused by an oxide layer on their surface, thus protecting the bimetallic core from oxidation.[14] This amorphous oxide layer mostly consists of alumina and iron oxide.[25] Potential applications for Fe/Al alloys include heating elements, insulation, tools, textiles, use as pipe material and hot gas filtration.[24] Yet, further applications of Fe/Al materials are very limited as they exhibit a poor room-temperature ductility, low high-temperature strength and strong embrittlement caused by reactions with water vapor.[24]

Kim *et al.* have shown that FeAl NPs can positively influence the otherwise low ductility of aluminum steel by using them as a second phase in the Al-rich steel when precipitated at grain boundaries and shear bands. As a result, the steel becomes

[a]*Institut für Anorganische Chemie und Strukturchemie, Heinrich-Heine-Universität Düsseldorf, 40204 Düsseldorf, Germany. E-mail: janiak@uni-duesseldorf.de; Fax: +49-211-81-12287; Tel: +49-211-81-12286*

[b]*Materials Discovery and Interfaces, Institut für Werkstoffe, Fakultät für Maschinenbau, Ruhr-Universität Bochum, Universitätsstr. 150, D-44801 Bochum, Germany*

[c]*Max-Planck-Institut für Eisenforschung GmbH, Max-Planck-Straße 1, D-40237 Düsseldorf, Germany*

[d]*Max-Planck-Institut für Chemische Physik fester Stoffe, Nöthnitzer Straße 40, D-01187 Dresden, Germany*

[e]*Department of Chemistry, Technische Universität München, D-85748 Garching, Germany*

† Electronic supplementary information (ESI) available: Synthesis of ionic liquids, details of bottom-up and top-down synthesis of Fe/Al NPs with their analysis. See DOI: 10.1039/d0ra01111h

Open Access Article. Published on 31 March 2020. Downloaded on 2/6/2026 9:28:58 AM.
This article is licensed under a Creative Commons Attribution-NonCommercial 3.0 Unported Licence.

stronger because the NPs facilitate shearing akin to a ball bearing.[26] Deevi *et al.* have shown that in microstructured alloys with the size of 4–10 μm the mechanical properties of the material can be enhanced in terms of room-temperature ductility and high temperature strength.[27] Accordingly, these results as well as catalytic applications of iron aluminides indicate a high interest in the systematic synthesis of well-defined Fe/Al NPs.

In general, NPs can be synthesized either by bottom-up or top-down processes. Bottom-up processes, in which NPs are generated by the reduction or decomposition of metal precursors, allow to achieve a variety of different NPs[28–32] but are accompanied by the drawback of by-products from the decomposition.[33] In the case of iron aluminide NPs an additional fundamental problem of such a synthetic approach is the formation of stable iron-centered clusters even at low Fe concentration, which suppresses the nucleation process and thus, the growth of crystalline particles.[34] Therefore, even larger concentrations of Fe led to amorphous nanomaterials, which may be interesting in terms of catalysis but are much more difficult to analyze.[34] Dutta *et al.* and Pithawalla *et al.*, who described the wet-chemical synthesis of FeAl or $Fe_3AlC_{0.5}$ nanoparticles by reducing anhydrous iron(II) chloride with lithium aluminum hydride, showed that a subsequent thermal treatment at temperatures of over 500 °C is required for the crystallization of the initial amorphous material.[35,36]

Therefore, ball-milling, as a top-down process, is the most reported way for the preparation of Fe/Al NPs.[36,37] This rather time-consuming method, however, leads to a relatively high number of defects and an often very wide particle size distribution in addition to particle impurities.[22,37] As a result, other synthetic methods have to be used to achieve high quality Fe/Al NPs. An example of this is the laser vaporization-controlled condensation (LVCC) method. Here, a macroscopic Fe/Al alloy is vaporized with a laser and subsequently, the vapor is condensed in a controlled manner in order to achieve a narrow particle size distribution and high purity.[22,35] For smaller batch sizes on a laboratory scale, the LVCC method is well suited, but not for desired larger industrial scales.[36] Hence, the controlled synthesis of defined Fe/Al NPs, possibly even as dispersion in a liquid medium, remains a challenge.

In this work we aimed for the synthesis of Fe/Al NPs *via* bottom-up and top-down processes, whereby the synthesis was performed either by soft wet-chemical reaction of organometallic precursors in ionic liquids (ILs) or by co-sputter deposition from respective metal targets into the ILs. The use of ILs for the stabilization of NPs as dispersion has proven to be promising in numerous cases.[38–43] ILs offer unique stabilizing properties for NPs due to their high polarity, dielectric constant, thermal stability, relatively low chemical reactivity.[44–46] Especially since no further additives (ligands, polymers, surfactants) are needed for the stabilization, and their negligible vapor pressure, ILs enable the sputter deposition of multinary NPs.[47]

## Experimental section

### Materials

All synthesis experiments were carried out under nitrogen or argon atmosphere using Schlenk techniques, since the organometallic precursors and the NPs are air and moisture sensitive. Solvents were dried using an MBRAUN solvent purification system and stored over molecular sieves. The acetonitrile (ACN) used for the NP precipitation was dried, degassed and stored under nitrogen. Lithium aluminum hydride (95%), lithium bis(trimethylsilyl)amide, iron(II) chloride (98%) and iron pentacarbonyl were obtained from Sigma Aldrich, diiron nonacarbonyl (99%) from abcr chemicals. All commercial chemicals were used without further purification. The precursors $(AlCp^*)_4$ (ref. 48) and $(CO)_4FeAlCp^*$ (ref. 49) were prepared according to literature.

**Lithium iron(II) bis(trimethylsilyl)amide, [LiFe(btsa)$_3$].** Lithium bis(trimethylsilyl)amide (1.26 g, 7.5 mmol) and iron(II) chloride (0.48 mg, 3.75 mmol) were reacted in molten lithium bis(trimethylsilyl)amide (mp 83–86 °C) without solvent at 90 °C in argon (Ar) atmosphere for 2 h (Scheme 1). Excess lithium bis(trimethylsilyl)amide was removed from the reaction mixture by sublimation at 60 °C ($1 \times 10^{-3}$ mbar) and subsequently the iron(II) bis(trimethylsilyl)amide was sublimed at 120 °C ($1 \times 10^{-3}$ mbar). $^1$H-NMR ($C_6D_6$, 300 MHz, 298 K): $\delta = 0.14$ (s, $Si(CH_3)_3$). $^{13}$C-NMR ($C_6D_6$, 75 MHz, 298 K): $\delta = 2.38$ (Fe–$N(Si(CH_3)_3)_2$–Li), 4.77 (Fe–$N(Si(CH_3)_3)_2$).

**IL synthesis.** The ILs were synthesized following established literature procedures. 1-Butyl-3-methylimidazolium bis(trifluoromethylsulfonyl)imide [BMIm][$NTf_2$] was obtained from the reaction of 1-methylimidazole and 1-chlorobutane to yield [BMIm][Cl] followed by anion exchange with $LiNTf_2$. 1-Butylpyridinium bis(trifluoromethylsulfonyl)imide [BPy][$NTf_2$] and 1-octylpyridinium bis(trifluoromethylsulfonyl)imide [OPy][$NTf_2$] were synthesized by reacting pyridine with 1-chlorobutane and 1-chlorooctane to yield [BPy][Cl] and [OPy][Cl], respectively followed by anion exchange with $LiNTf_2$ (Scheme S1†).[50] The syntheses for the chloride intermediates were carried out in a Mars 6 microwave (CEM). For [BMIm][Cl] the reaction temperature was 160 °C and for [OPy][Cl] and [BPy][Cl] 180 °C, which was kept for 1 h.[51] The final $NTf_2$-ILs were dried under high vacuum at 80 °C for two days. Anion purity was assessed by ion chromatography (Dionex ICS-1100, with IonPac® AS22, 4 × 250 mm column) to be >99% following a published procedure.[50] Water content was measured by coulometric Karl Fischer titration (ECH/ANALYTIK JENA AQUA 40.00) (<10 ppm).

**Bottom-up NP synthesis.** All precursor decomposition reactions induced by microwave heating were carried out under Ar atmosphere. Amounts of the organometallic precursors were set to yield 1.0 wt% dispersions of Fe/Al NPs in IL (Table 1). The precursor-IL dispersion was stirred for 24 h and then brought to

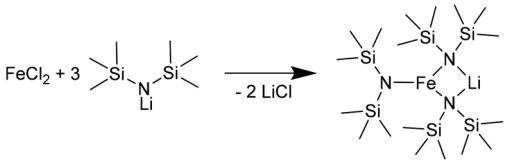


Scheme 1 Synthesis of [LiFe(btsa)$_3$] from lithium bis(trimethylsilyl) amide and iron(II) chloride.

 This journal is © The Royal Society of Chemistry 2020

Open Access Article. Published on 31 March 2020. Downloaded on 2/6/2026 9:28:58 AM.
This article is licensed under a Creative Commons Attribution-NonCommercial 3.0 Unported Licence.

Table 1 Starting amounts of precursors for wet chemical synthesis approaches

| Ionic liquid [g] | | Fe-Precursor [mg] (Fe[a] [mmol]) | | Al-Precursor [mg] (Al[a] [mmol]) | |
|---|---|---|---|---|---|
| [OPy][$NTf_2$] | 1.02 | $FeCl_2$ | 23 (0.22) | $LiAlH_4$ | 8 (0.18) |
| [OPy][$NTf_2$] | 1.01 | [$LiFe(btsa)_3$] | 97 (0.18) | $LiAlH_4$ | 8 (0.18) |
| [BMIm][$NTf_2$] | 1.02 | $Fe(CO)_5$ | 24 (0.12) | $(AlCp^*)_4$ | 21 (0.13) |
| [BMIm][$NTf_2$] | 1.1 | $Fe_2(CO)_9$ | 22 (0.12) | $(AlCp^*)_4$ | 21 (0.13) |

| Ionic liquid [g] | | Fe/Al-precursor [mg] (Fe and Al each [mmol]) | |
|---|---|---|---|
| [BMIm][$NTf_2$] | 1.01 | $(CO)_4FeAlCp^*$ | 20 (0.06) |

[a] Fe and Al [mmol] refer to the metal amount and were set for the intended molar 1 : 1 Fe : Al ratio.

reaction by microwave-induced heating (CEM, Discover microwave, max. 50 W) for 30 min at 170 °C for $FeCl_2/LiAlH_4$ and for 30 min at 230 °C for the other precursors (Table 1). After the synthesis the NPs were precipitated from the IL dispersion with 3 mL of ACN, separated by centrifugation (Hettich Zentrifuge, 6000 U $min^{-1}$ for 20 min), washed up to five times or until the washing solution remained colorless with 3 mL each of ACN. The resulting black materials were dried under high vacuum. If the resulting product was still lumpy, the sample was washed again with ACN.

**Top-down NP synthesis.** The sputter targets were received from EvoChem and each had a purity of 99.99%. The synthesis was performed in a magnetron sputter system (AJA POLARIS-5 chamber) with 1.5-inch diameter cathodes and a direct current (DC) power supply. Ar was used as process gas with a purity of 99.999%.

A multiple cavity holder was applied for sputtering into the ILs with a volume of 35 μL per cavity as described elsewhere.[47] With special designed covers, between 6 or a maximum of 64 cavities are available (Fig. 1). For cleaning, the holder was ultrasonicated 20 minutes each in technical-grade acetone and isopropanol. The cavities were filled with the ILs [BMIm][$NTf_2$], [OPy][$NTf_2$], [BPy][$NTf_2$] under Ar atmosphere (Fig. 1). Pieces of a patterned $Si/SiO_2$ wafer (2 cm × 3 cm), photolithographically structured with a photoresist lift-off cross pattern for film thickness determination, were placed in each quadrant of the cavity holder (Fig. 1).

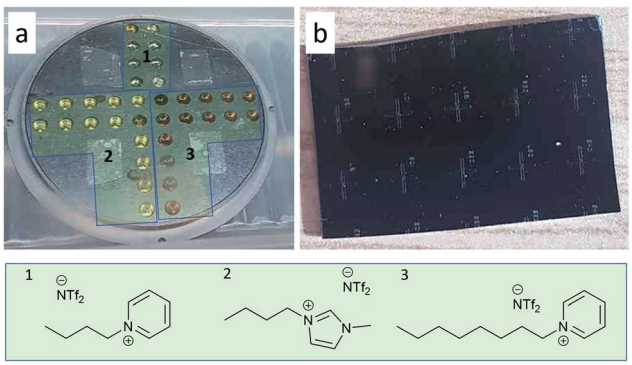


Fig. 1 (a) Cavity holder for the DC-sputter deposition with ILs in cavities, photo taken after Fe/Al sputter deposition into three different ILs (with IL regions marked 1–3). The lighter areas in the four quadrants are regions where the $Si/SiO_2$ wafer pieces were attached (photo taken after removal). (b) $Si/SiO_2$ wafer piece also showing the cross-patterned reference regions for film thickness determination.

The as-such prepared cavity-holder was stored in the vacuum chamber overnight under a vacuum of $1.3 \times 10^{-4}$ Pa. DC sputter deposition of Fe/Al NPs was performed as follows: After filling with Ar to a pressure of 1.33 Pa and plasma ignition at 20 W for a 2 min precleaning step, the Ar pressure was reduced to 0.5 Pa. A cathode tilt of 12° relative to the normal of the cavity holder was used for deposition (Fig. S1, ESI†). The deposition was performed at 25 W (305 V, 82 mA) for Fe and 46 W (342 V, 134 mA) for Al over a period for 2 h. After sputter deposition, the holder was removed and transported under Ar atmosphere to a glove box. There the NP/IL dispersions were collected and stored under Ar in the glove box.

## Methods

**Bottom-up samples.** High-resolution transmission electron microscopy (HR-TEM) imaging of the precipitated, separated and washed bottom-up samples was performed on a FEI Tecnai G2 F20 electron microscope (Gemeinschaftslabor für Elektronenmikroskopie RWTH-Aachen, Ernst Ruska-Centrum für Mikroskopie und Spektroskopie mit Elektronen, Jülich) operated at 200 kV accelerating voltage.[52] Digital images were recorded by a Gatan UltraScan 1000P detector. Samples were prepared using 200 μm carbon-coated copper or gold grids. Energy-dispersive X-ray spectroscopy (EDX) spectroscopy was also performed on the FEI Tecnai G2 F20 with a high angle energy dispersive X-ray detector providing a resolution of 136 eV or better for Mn K-α radiation. The exposure time of individual EDX spectra was 3 min.

Thermal analyses were performed on a NETZSCH TG Tarsus 209 F3 with a heating rate of 5 K $min^{-1}$ under $N_2$ atmosphere up to a temperature of 1000 °C.

Atomic absorption spectroscopy (AAS) for metal analysis were performed on a PerkinElmer PinAAcle 900T, equipped with flame and graphite furnace and with automatic sampler for the graphite-furnace mode. This AAS instrument has a transversely heated graphite atomizer with longitudinal Zeeman-effect background correction. Flame-AAS was used for Fe and graphite-furnace AAS for Al. Samples were digested in hot *aqua regia* two times. The residues were re-dissolved in *aqua regia* (8 mL), filtered and brought with water to a total volume of 50 mL. For the iron measurements the samples were diluted 1 : 10 and for aluminum 1 : 100.

Scanning-electron microscope (SEM) images were recorded with a JEOL JSM-6510LV QSEM advanced electron microscope equipped with a $LaB_6$ cathode. The microscope was equipped with a Bruker Xflash 410 silicon drift detector and Bruker ESPRIT software for EDX analysis. The samples were prepared for SEM microscopy by coating them with gold using a JEOL JFC 1200 fine-coater. The samples were placed on brass sample holders fixed with a carbon tape.

Open Access Article. Published on 31 March 2020. Downloaded on 2/6/2026 9:28:58 AM. This article is licensed under a Creative Commons Attribution-NonCommercial 3.0 Unported Licence.

Powder X-ray diffractometry (PXRD) were measured at ambient temperature on a Bruker D2 Phaser using a flat sample holder and Cu Kα radiation ($\lambda = 1.54182$ Å, 35 kV). PXRDs were measured for 30 min.

**Top-down samples.** The thin film on the $Si/SiO_2$ wafer was analyzed by EDX (Oxford INCA XAct SiLi detector) in a SEM (JEOL JSM-5800 LV) and revealed a composition of Al 76 at% and Fe 24 at%.

Initial characterization of the NP/IL dispersion from DC sputter deposition was performed with a FEI Tecnai F20 S/TEM (Institut für Werkstoffe, Fakultät für Maschinenbau, Ruhr-Universität Bochum). For these TEM investigations a holey carbon-coated gold grid (200 mesh) was used and 2.5 μL of the NP/IL sample was dropped on the C-coated side and left for NP adhesion for 2 h. Dried ACN was used to wash the grid dropwise for 1 h under inert conditions. The grid was stored in Ar atmosphere. Further information can be found elsewhere.[47]

The as-deposited NPs in the ILs were crystallized *ex situ* under vacuum (30 Pa) at 100 °C for 2, 5 and 10 h in a silicone oil bath and then cooled down to room temperature in order to verify a possible crystallization.

HR-TEM characterization of the sputter-deposited and heat-treated sample in $[OPy][NTf_2]$ for 10 h was performed in a Titan Themis 60-300 X-FEG (Max-Planck-Institut für Eisenforschung GmbH, Düsseldorf) equipped with an image corrector, operated at 300 kV. TEM images were recorded on a metal-oxide-semiconductor (CMOS) camera with 4k · 4k pixels. Beam-induced *in situ* crystallization was achieved at 300 kV with a dose rate $\sim 6 \times 10^5$ e nm$^{-2}$ s$^{-1}$, for a total time of 30 min, with a magnification of 490 k×, spot size 3 and a screen current of 9.47 nA.

HR-TEM analysis was also carried out by the FEI Tecnai F30-G2 (Max-Planck-Institut für Chemische Physik fester Stoffe, Dresden) with super-twin and a field emission gun at an acceleration voltage of 300 kV. The point resolution amounted to 2.0 Å, and the information limit amounted to about 1.2 Å. The microscope is equipped with a slow scan CCD camera (MultiScan, 2k·2k pixels; Gatan Inc., Pleasanton, CA, USA).

X-ray photoelectron spectroscopy (XPS) was performed with an ULVAC-PHI VersaProbe II microfocus X-ray photoelectron spectrometer. The spectra were recorded using a polychromatic aluminum Kα X-ray source (1486.8 eV) and referenced to the carbon 1s orbital with a binding energy of 284.8 eV. Fitting of the experimental XP spectra was done with the program CasaXPS (version 2.3.19PR1.0, copyright 1999–2018, Casa Software Ltd).

## Results and discussion

The synthesis of iron aluminide alloy NPs was attempted from different Fe and Al starting materials by two methods and in three ILs with an overview given in Table 2. The three ILs $[BMIm][NTf_2]$, $[BPy][NTf_2]$ and $[OPy][NTf_2]$ (Fig. 1, Scheme S1†) were used for the Fe/Al nanoparticle syntheses. The $[NTf_2]^-$ anion was chosen because of its hydrophobic character and its hydrothermal stability, since the anion $[BF_4]^-$ is well known to form metal-fluoride nanoparticles.[53,54]

The IL cations can have a profound effect on the stabilization, size and size distribution of the obtained metal nanoparticles.[55,57] Imidazolium-ILs, in particular with the cation $[BMIm]^+$ are well established for the synthesis of small NPs.[18,19,54,56–60] However, $[BMIm]^+$ contains a slightly acidic proton in the C-2 position which can lead to metal-carbene formation.[61] The cation $[BPy]^+$ was included here because of the absence of such acidic protons. The cation $[OPy]^+$ was used because it is even more hydrophobic than $[BPy]^+$ and offers a better steric stabilization of the nanoparticles through its long alkyl chain.[18]

### Bottom-up approach

Generally, our bottom-up soft wet-chemical syntheses of Fe/Al NPs in ILs yielded crystalline FeAl NPs either agglomerated or only together with an amorphous background.

Following the literature,[22,24,35,36] first iron(II) chloride and lithium aluminum hydride were suspended in IL and reacted by microwave irradiation (Fig. S2†). According to the TEM images, EDX analyses and PXRD, strongly agglomerated but crystalline FeAl NPs could be found together with amorphous regions (Fig. S3†). The latter probably consist of amorphous aluminum and iron oxides, which is confirmed by a distinct oxygen signal in the EDX spectra. Since it is known that the presence of halide anions (here from $FeCl_2$) induces the agglomeration of NPs, other synthetic routes were pursued.[62]

Kelsen *et al.* and Amiens *et al.* were able to produce small pure Fe NPs by hydrogenation of bis[bis(trimethylsilyl)amido] iron(II) $[[Fe(btsa)_2]_2]$.[63,64] Our reaction of $[LiFe(btsa)_3]$ with $LiAlH_4$ (Fig. S4†) led to crystalline FeAl NPs on an amorphous background (SAED in Fig. S5, ESI†). We note that the btsa ligand is decomposed by heating to 170 °C to volatile products, which can easily be removed from the reaction mixture.

Given the observed unsatisfactory results from the reduction of Fe(II) salts with $LiAlH_4$, we decided to follow a fully organometallic approach avoiding the addition of a separate reducing agent. Organometallic precursor compounds with labile ligands, *e.g.* with CO and Cp* (pentamethylcyclopentadienyl) have been frequently used successfully for the synthesis of metal NPs.[14,15,18,61,65–67] A recent related example was the synthesis of CoAl NPs from $Co_2(CO)_8$ and AlCp*.[20] Therefore, we applied this route to the synthesis of Fe/Al NPs through the reaction of the iron carbonyls $[Fe(CO)_5$ or $Fe_2(CO)_9]$ and AlCp*(Fig. S6 and S8†). In case of $Fe(CO)_5$, small $FeAl_2O_4$ NPs could be identified which are immobilized on an amorphous background material (SAED in Fig. S7, ESI†). From the reaction with $Fe_2(CO)_9$ only amorphous products could be found according to PXRD, EDX and FFT analyses (Fig. S9, ESI†).

The above dual-source approaches were complemented by a single-source approach using the intermetallic complex $(CO)_4$FeAlCp* (Fig. S10, ESI†). The formation of bimetallic FeAl NPs should be promoted by the already existing intermetallic Fe–Al bond.[68,69] Yet, the decomposition of $(CO)_4$FeAlCp* (ref. 49) yielded only amorphous phases (Fig. S11, ESI†) as seen before in the dual source approach with $Fe_2(CO)_9$ and AlCp*.

The bottom-up NP/IL samples were also analyzed by TGA, AAS and SEM-EDX for the amount of metal and content of the

 This journal is © The Royal Society of Chemistry 2020

Open Access Article. Published on 31 March 2020. Downloaded on 2/6/2026 9:28:58 AM. This article is licensed under a Creative Commons Attribution-NonCommercial 3.0 Unported Licence.

Table 2 Overview of Fe/Al NP products from different synthesis routes in this work[a]

| Method | Ionic liquid | Metal source | Crystalline phase[b] | Size [nm] |
|---|---|---|---|---|
| Bottom-up | $[OPy][NTf_2]$ | $FeCl_2$, $LiAlH_4$ | FeAl | —[c] |
| | | $[LiFe(btsa)_3]$, $LiAlH_4$ | FeAl | $10 \pm 2$[d] |
| | $[BMIm][NTf_2]$ | $Fe(CO)_5$, $(AlCp^*)_4$ | $FeAl_2O_4$ | $1.0 \pm 0.5$[d] |
| | | $Fe_2(CO)_9$, $(AlCp^*)_4$ | None | —[c] |
| | | $(CO)_4FeAlCp^*$ | None | —[c] |
| Top-down | $[OPy][NTf_2]$ | Fe, Al target | $Fe_4Al_{13}$[e] | 2–4[f] |
| | $[BPy][NTf_2]$ | | n.a.[g] | 2–4[f] |
| | $[BMIm][NTf_2]$ | | n.a.[g] | 2–4[f] |

[a] 1 wt% metal-NP/IL dispersions obtained by microwave-assisted heating for 30 min at 230 °C. [b] The identity of the crystalline fraction of NPs was determined by powder X-ray diffractometry (PXRD), selected area electron diffraction (SAED) or fast Fourier transformation (FFT) in the TEM. [c] No separated particles were found. [d] Average diameter (Ø). See Experimental section for transmission electron microscopy (TEM) measurement conditions, at least 100 particles were used for the size analysis. [e] Phase determination after 10 h annealing at 100 °C. [f] Range of particle size from various TEM images. [g] n.a. = not available but the same synthesis conditions as for the sample in $[OPy][NTf_2]$ were used, albeit without annealing so that the low crystallinity prevented a phase determination.

adhering IL. This composition analysis showed more than 50 wt% of IL still adhering to the precipitated, separated and washed samples from the NP/IL dispersions. At the same time the Fe : Al ratio deviated from the 1 : 1 expectation (Fig. S12–S15, Table S1 and S2, ESI†).

In summary, the attempted synthesis of the Fe/Al NPs in ILs using a bottom-up method yielded unclear samples with a presumably amorphous metal-oxide background.

### Top-down approach

As a top-down method, magnetron co-sputtering using elemental metal targets and Ar as sputter gas enables the synthesis of multinary NPs libraries without limits, *e.g.* related to the chemical reactivity of the used metal precursors.[47,70,71] This approach has led to the discovery of noble metal free eletrocatalysts.[71–73]

The synthesis of the Fe/Al NPs was carried out in a commercial co-sputter system with 1.5-inch diameter magnetron sputter cathodes using DC power on the Fe and Al targets. A cavity holder was used for the deposition of metals into ILs (Fig. 1a). Each cavity was filled with 35 μL of IL. Next to the cavities, photolithographically structured wafer pieces were placed on the cavity holder lid for the thin film analysis (Fig. 1b).

The chemical composition of the thin films on the Si wafer piece was analyzed by SEM-EDX on the patterned reference regions of the $Si/SiO_2$ wafer to yield a composition of 24 at% Fe and 76 at% Al. However, the composition of the thin film and the NPs can deviate.[74]

XPS analysis of the film on the Si substrate was done for further compositional analysis (Table S3, Fig. S16–S18, ESI†). The XPS survey spectrum (Fig. S16, ESI†) identifies aluminum, carbon, silicon, oxygen and iron in the sputtered sample in $[OPy][NTf_2]$. The O 1s orbital indicates two different oxygen species (Table S3 and Fig. S18, ESI†). The first species at 530.7 eV can be ascribed to a metal oxide and the second at 532.0 eV to $SiO_2$.[75] The Al 2p orbital binding energy of 74.3 eV indicates $Al_2O_3$ (ref. 75) and at 72.0 eV $Al^0$.[76] For the Fe $2p_{3/2}$ orbital the binding energy at 706.2 eV can be assigned to $Fe^0$ and the bands between 707.1 eV and 710.1 eV to a mixture of $Fe^{II}$ and $Fe^{III}$.[77]

A possible partial oxidation of the sample before XPS cannot be excluded. The reason is a contact with air after the synthesis to transfer the samples into the glovebox. Since XPS is very surface-sensitive, it shows an oxidation of the Fe/Al film. The quantification of Fe and Al over the entire substrate gave a Fe : Al molar ratio of 1 : 3 in agreement with the EDX results.

Fig. 2 shows the NPs/IL suspensions directly after the magnetron sputter synthesis. All NPs have a size between 2 and 4 nm as determined from TEM images (Fig. 4a, b, S19 and S23, ESI†).

We exemplarily describe here the analysis of the Fe/Al NPs obtained from the magnetron sputter synthesis in $[OPy][NTf_2]$. For the characterization of the samples in $[BMIm][NTf_2]$ and $[BPy][NTf_2]$ see ESI (Fig. S19–S23†).

The sputtered Fe/Al NPs in $[OPy][NTf_2]$ showed an unexpected red color, which remained after thermal annealing (*vide infra*) and which was examined by UV-vis spectroscopy (Fig. 2c and 3). The NPs in the $[OPy][NTf_2]$ IL exhibit two absorption bands in the green-blue to green spectral region at 475 and 520 nm which give rise to the complementary red color. This absorption maximum at 520 nm and the resulting red color is akin to the surface plasmon resonance of Au NPs,[78]

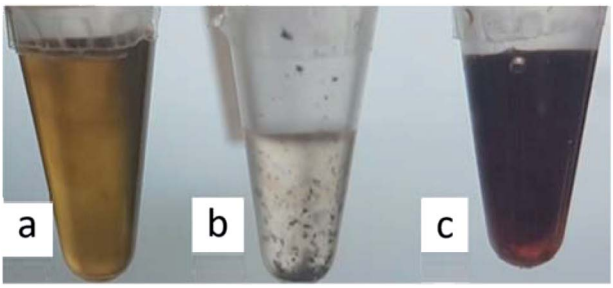


Fig. 2 Magnetron sputter synthesized Fe/Al NPs dispersions, (a) in $[BMIm][NTf_2]$, (b) in $[BPy][NTf_2]$ and (c) in $[OPy][NTf_2]$ in 1.5 mL Eppendorf caps.

Open Access Article. Published on 31 March 2020. Downloaded on 2/6/2026 9:28:58 AM.
This article is licensed under a Creative Commons Attribution-NonCommercial 3.0 Unported Licence.

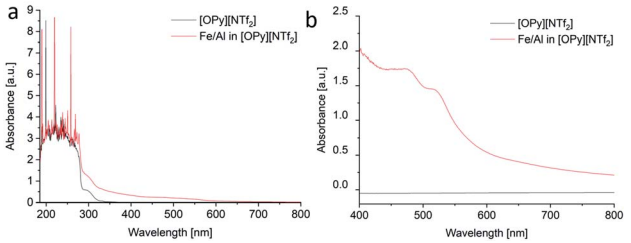


Fig. 3 (a and b) UV-vis spectra from the Fe/Al NP/IL dispersion in [OPy][$NTf_2$] measured over different wavelength regions.

which suggest that Fe/Al NPs of the right size mimic the electronic surface structure of Au NPs including a similar band gap width.[79] At present there are limited reports on the electronic band structure of bulk Fe/Al alloys[80] but none on the nanoscale. Even for Au NPs accurate computational approaches with good agreement to experiments and a correct description of the electronic situation appears still challenging.[78,81]

The characterization of Fe/Al NPs in [OPy][$NTf_2$] by TEM indicated the formation of small NPs together with amorphous material (Fig. 4). The elemental analysis from the EDX spectrum of the image region gives a Fe : Al molar ratio of 20 : 80. When sample areas with a large amount of amorphous material were investigated in the TEM, crystalline NPs were spontaneously formed under the electron beam.[82] In order to promote the crystallization of the NPs outside of the TEM, the Fe/Al@[OPy][$NTf_2$] sample was heated (annealed) for altogether 10 h at

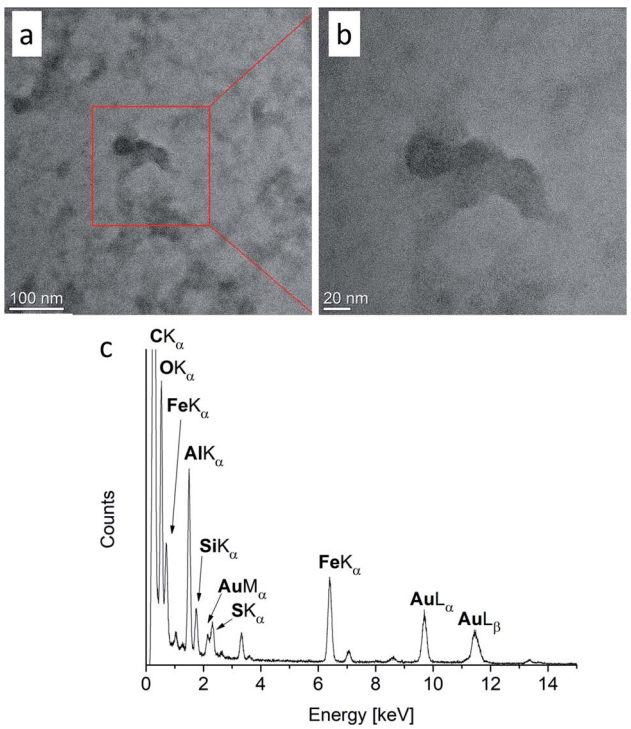


Fig. 4 (a and b) TEM images of Fe/Al NPs sputtered in [OPy][$NTf_2$] (c) EDX spectrum of the image region of (b). The EDX spectrum shows the remains of adhering IL with the sulfur signal originating from the IL anion. Au and C signals in the EDX are caused by the TEM grid.

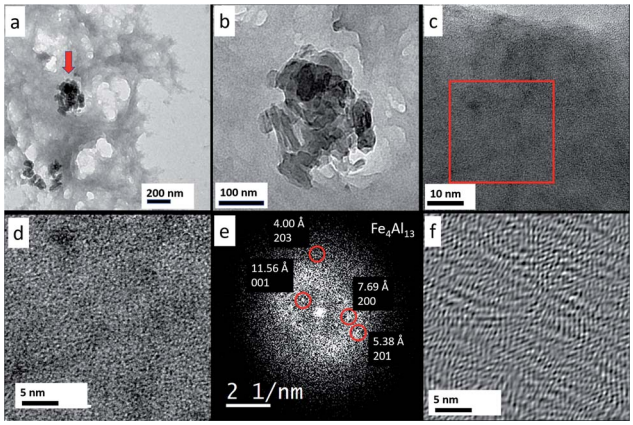


Fig. 5 (a) Overview TEM micrograph of Fe/Al NPs (see red arrow) embedded in the IL [OPy][$NTf_2$]. (b) Zoom shows that the aggregate consists of NPs. (c) Further enlargement reveals that the NPs consist of an amorphous matrix. (d) At atomic resolution, poor crystallinity is observed. (e) Fast Fourier transform (FFT) of (d) shows weak reflections, which agree to a $Fe_4Al_{13}$ lattice. (f) FFT filtered image of (d) displaying distorted crystal lattices.

100 °C in vacuum (see ESI for analyses of intermediate annealing times with Fig. S24 and S25†).[47]

After a total annealing time of 10 h, embedded Fe/Al nanoaggregates in the ionic liquid matrix (Fig. 5a and b) were

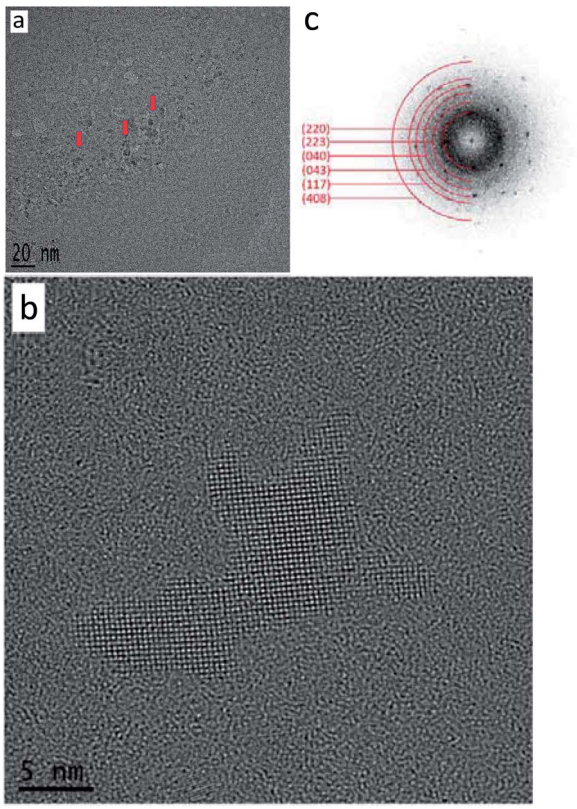


Fig. 6 (a) Overview TEM image of electron beam crystallized Fe/Al NPs (indicated by red arrows) in the IL [OPy][$NTf_2$]. (b) HRTEM of a single particle. (c) FFT of the NPs and the assignment based on the ICSD 151129 for (bulk) $Fe_4Al_{13}$.


This journal is © The Royal Society of Chemistry 2020

Open Access Article. Published on 31 March 2020. Downloaded on 2/6/2026 9:28:58 AM.
This article is licensed under a Creative Commons Attribution-NonCommercial 3.0 Unported Licence.

Table 3 Comparison of the theoretical *d*-spacing values with the measured ones

| *d*-Spacing reference[a] (*hkl*) | *d*-Spacing measured |
|---|---|
| 3.54 (220) | 3.53 |
| 2.46 (223) | 2.48 |
| 2.01 (040) | 2.01 |
| 1.79 (043) | 1.77 |
| 1.59 (117) | 1.58 |
| 1.25 (408) | 1.24 |

[a] For bulk $Fe_4Al_{13}$ ICSD: 151129.

susceptible to fast Fourier transform (FFT) analysis of the HR-TEM images (Fig. 5e) and gave a clear indication of a $Fe_4Al_{13}$ phase (see ESI, Fig. S26 and S27† for further HR-TEM images from other sample areas with FFT analysis and $Fe_4Al_{13}$ phase assignment).

Also, the Fe/Al NPs were continued to be crystallized *in situ* in the HR-TEM at 300 kV and a magnification of 490 kx. Every 10 minutes a picture was taken (Fig. S28, ESI†) and a FFT was generated to verify the crystallinity of the NPs. After 30 min sufficiently crystalline NPs could be obtained (Fig. 6a and b).

From the sample an FFT was generated and the reflexes could be assigned to the $Fe_4Al_{13}$ phase with the space group *C*12/*m*1 (Table 3 and Fig. 6c).

## Conclusions

We prepared Fe/Al NPs *via* a bottom-up and a top-down approach. The bottom-up approach yielded FeAl NPs, albeit with an amorphous background from the dual-source approach with $FeCl_2$ and $LiAlH_4$ or with $[LiFe(btsa)_3]$ and $LiAlH_4$. Very small Fe/Al NPs from the dual-source approach with the iron carbonyl $Fe(CO)_5$ and $(AlCp^*)_4$ were apparently almost completely oxidized and analyzed as $FeAl_2O_4$ NPs. The top-down synthesis by magnetron co-sputtering using elemental metal targets and Ar yielded very small $Fe_4Al_{13}$ NPs with a size of 2–4 nm. Unequivocal phase determination was possible after thermal and electron-beam annealing which was exemplarily carried out in the ionic liquid $[OPy][NTf_2]$. The Fe/Al NPs in $[OPy][NTf_2]$ showed a red color, before and after thermal annealing and the absorption maximum in the visible region at 520 nm is akin to the plasmon resonance of Au NPs, which suggests a similar electronic structure for both Fe/Al and Au NPs. We will continue to investigate the properties of Fe/Al NPs in further studies.

## Conflicts of interest

There are no conflicts to declare.

## Acknowledgements

This work has been supported by the German Science Foundation (DFG) within the priority program SPP 1708 "Material Synthesis Near Room Temperature" (grant JA 466/31-1/2 for C. J., grant Fi502/32-1/2 for R. A. F) and by the BMBF project NEMEZU. M. M. and A. L. acknowledge DFG funding of the project LU1175/23-1. A. G. M. and C. S. acknowledge DFG funding of the project SCHE 634/21-1. We thank Mr Tim-Oliver Knedel for the UV-vis spectra.

## Notes and references

1 P. Migowski and J. Dupont, *Chem.–Eur. J.*, 2007, **13**, 32–39.
2 J. Conde, G. Doria and P. Baptista, *J. Drug Delivery*, 2012, **2012**, 751075.
3 Q. A. Pankhurst, J. Connolly, S. K. Jones and J. Dobson, *J. Phys. D: Appl. Phys.*, 2003, **36**, R167.
4 A. L. Stepanov, in *Glass Nanocomposites*, ed. B. Karmakar, K. Rademann and A. L. Stepanov, William Andrew Publishing, Boston, 2016, pp. 165–179.
5 M. Li, S. K. Cushing and N. Wu, *Analyst*, 2014, **140**, 386–406.
6 W. Wu, *Nanoscale*, 2017, **9**, 7342–7372.
7 J. D. Scholten, B. C. Leal and J. Dupont, *ACS Catal.*, 2012, **2**, 184–200.
8 W. J. Stark, P. R. Stoessel, W. Wohlleben and A. Hafner, *Chem. Soc. Rev.*, 2015, **44**, 5793–5805.
9 P. M. Humbert and J. G. Chen, *J. Catal.*, 2008, **257**, 297–306.
10 M. Armbrüster, G. Wowsnick, M. Friedrich, M. Heggen and R. Cardoso-Gil, *J. Am. Chem. Soc.*, 2011, **133**, 9112–9118.
11 R. Hudson, C.-J. Li and A. Moores, *Green Chem.*, 2012, **14**, 622–624.
12 H. L. Ngyuen, L. E. M. Howard, S. R. Giblin, B. K. Tanner, I. Terry, A. K. Hughes, I. M. Ross, A. Serres, H. Bürckstümmer and J. S. O. Evans, *J. Mater. Chem.*, 2005, **15**, 5136–5143.
13 Y. Chen, X. Luo, G.-H. Yue, X. Luo and D.-L. Peng, *Mater. Chem. Phys.*, 2009, **113**, 412–416.
14 M. Cokoja, H. Parala, A. Birkner, R. A. Fischer, O. Margeat, D. Ciuculescu, C. Amiens, B. Chaudret, A. Falqui and P. Lecante, *Eur. J. Inorg. Chem.*, 2010, 1599–1603.
15 M. Cokoja, H. Parala, A. Birkner, O. Shekhah, M. W. E. van Berg and R. A. Fischer, *Chem. Mater.*, 2007, **19**, 5721–5733.
16 M. Cokoja, H. Parala, M. K. Schröter, A. Birkner, M. W. E. van den Berg, W. Grünert and R. A. Fischer, *Chem. Mater.*, 2006, **18**, 1634–1642.
17 M. Cokoja, B. J. Jagirdar, H. Parala, A. Birkner and R. A. Fischer, *Eur. J. Inorg. Chem.*, 2008, 3330–3339.
18 K. Schütte, A. Doddi, C. Kroll, H. Meyer, C. Wiktor, C. Gemel, G. van Tendeloo, R. A. Fischer and C. Janiak, *Nanoscale*, 2014, **6**, 5532–5544.
19 K. Schütte, H. Meyer, C. Gemel, J. Barthel, R. A. Fischer and C. Janiak, *Nanoscale*, 2014, **6**, 3116–3126.
20 L. Schmolke, B. Gregori, B. Giesen, A. Schmitz, J. Barthel, L. Staiger, R. A. Fischer, A. J. von Wangelin and C. Janiak, *New J. Chem.*, 2019, **43**, 16583–16594.
21 M. Armbrüster, K. Kovnir, M. Friedrich, D. Teschner, G. Wowsnick, M. Hahne, P. Gille, L. Szentmiklósi, M. Feuerbacher, M. Heggen, F. Girgsdies, D. Rosenthal, R. Schlögl and Y. Grin, *Nat. Mater.*, 2012, **11**, 690–693.

Open Access Article. Published on 31 March 2020. Downloaded on 2/6/2026 9:28:58 AM.
This article is licensed under a Creative Commons Attribution-NonCommercial 3.0 Unported Licence.

22 Y. B. Pithawalla, M. S. El Shall and S. C. Deevi, *Intermetallics*, 2000, **8**, 1225–1231.
23 C. T. Liu, E. P. George, P. J. Maziasz and J. H. Schneibel, *Mater. Sci. Eng., A*, 1998, **258**, 84–89.
24 Y. B. Pithawalla, M. S. El-Shall, S. C. Deevi, V. Ström and K. V. Rao, *J. Phys. Chem. B*, 2001, **105**, 2085–2090.
25 T. Liu, Y. Pang, H. Kikuchi, Y. Kamada and S. Takahashi, *J. Mater. Chem. C*, 2015, **3**, 6232–6239.
26 S.-H. Kim, H. Kim and N. J. Kim, *Nature*, 2015, **518**, 77–79.
27 S. C. Deevi, V. K. Sikka and C. T. Liu, *Prog. Mater. Sci.*, 1997, **42**, 177–192.
28 P. Migowski, G. Machado, S. R. Texeira, M. C. M. Alves, J. Morais, A. Traverse and J. Dupont, *Phys. Chem. Chem. Phys.*, 2007, **9**, 4814–4821.
29 C. C. Cassol, A. P. Umpierre, G. Machado, S. I. Wolke and J. Dupont, *J. Am. Chem. Soc.*, 2005, **127**, 3298–3299.
30 K.-S. Kim, D. Demberelnyamba and H. Lee, *Langmuir*, 2004, **20**, 556–560.
31 C. N. R. Rao, H. S. S. Ramakrishna Matte, R. Voggu and A. Govindaraj, *Dalton Trans.*, 2012, **41**, 5089–5120.
32 I. S. Helgadottir, P. P. Arquillière, P. Bréa, C. C. Santini, P.-H. Haumesser, K. Richter, A.-V. Mudring and M. Aouine, *Microelectron. Eng.*, 2003, **107**, 229–232.
33 T. Torimoto, K.-i. Okazaki, T. Kiyama, K. Hirahara, N. Tanak and S. Kuwabata, *Appl. Phys. Lett.*, 2006, **89**, 243117.
34 S. Xiao, X. Li, H. Deng, L. Deng and W. Hu, *Phys. Chem. Chem. Phys.*, 2015, **17**, 6511–6522.
35 D. P. Dutta, G. Sharma, A. K. Rajarajan, S. M. Yusuf and G. K. Dey, *Chem. Mater.*, 2007, **19**, 1221–1225.
36 Y. B. Pithawalla and S. Deevi, *Mater. Res. Bull.*, 2004, **39**, 2303–2316.
37 S. Mende, F. Stenger, W. Peukert and J. Schwedes, *Chem. Ing. Tech.*, 2002, **74**, 994–1000.
38 P. S. Campbell, M. H. G. Prechtl, C. C. Santini and P.-H. Haumesser, *Curr. Org. Chem.*, 2013, **17**, 414–429.
39 D. Freudenmann, S. Wolf, M. Wolff and C. Feldmann, *Angew. Chem., Int. Ed.*, 2011, **50**, 11050–11060.
40 E. Ahmed, J. Breternitz, M. F. Groh and M. Ruck, *CrystEngComm*, 2012, **14**, 4874–4885.
41 H. Kaper, F. Endres, I. Djerdj, M. Antonietti, B. M. Smarsly, J. Maier and Y.-S. Hu, *Small*, 2007, **3**, 1753–1763.
42 M. Antonietti, D. Kuang, B. Smarsly and Y. Zhou, *Angew. Chem., Int. Ed.*, 2004, **43**, 4988–4992.
43 D. Marquardt and C. Janiak, *Nachr. Chem.*, 2013, **61**, 754–757.
44 P. Wasserscheid and W. Keim, *Angew. Chem., Int. Ed.*, 2000, **39**, 3772–3789.
45 J. Dupont and J. D. Scholten, *Chem. Soc. Rev.*, 2010, **39**, 1780–1804.
46 C. S. Consorti, P. A. Z. Suarez, R. F. de Souza, R. A. Burrow, D. H. Farrar, A. J. Lough, W. Loh, L. H. M. da Silva and J. Dupont, *J. Phys. Chem. B*, 2005, **109**, 4341–4349.
47 H. Meyer, M. Meischein and A. Ludwig, *ACS Comb. Sci.*, 2018, **20**, 243–250.
48 C. Ganesamoorthy, S. Loerke, C. Gemel, P. Jerabek, M. Winter, G. Frenking and R. A. Fischer, *Chem. Commun.*, 2013, **49**, 2858–2860.
49 J. Weiss, D. Stetzkamp, B. Nuber, R. A. Fischer, C. Boehme and G. Frenking, *Angew. Chem., Int. Ed.*, 1997, **36**, 70–72.
50 C. Rutz, L. Schmolke, V. Gvilava and C. Janiak, *Z. Anorg. Allg. Chem.*, 2017, **643**, 130–135.
51 M. Deetlefs and K. R. Seddon, *Green Chem.*, 2003, **5**, 181–186.
52 Ernst Ruska-Centre for Microscopy and Spectroscopy with Electrons, FEI Tecnai G2 F20, *Journal of large-scale research facilities*, 2016, **2**, A77.
53 A. Schmitz, K. Schütte, V. Ilievski, J. Barthel, L. Burk, R. Mülhaupt, J. Yue, B. Smarsly and C. Janiak, *Beilstein J. Nanotechnol.*, 2017, **8**, 2474–2483.
54 M. Siebels, L. Mai, L. Schmolke, K. Schütte, J. Barthel, J. Yue, J. Thomas, B. M. Smarsly, A. Devi, R. A. Fischer and C. Janiak, *Beilstein J. Nanotechnol.*, 2018, **9**, 1881–1894.
55 P. Migowski, D. Zanchet, G. Machado, M. A. Gelesky, S. R. Teixeira and J. Dupot, *Phys. Chem. Chem. Phys.*, 2010, **12**, 6826–6833.
56 K. Klauke, I. Gruber, T.-O. Knedel, L. Schmolke, J. Barthel, H. Breitzke, G. Buntkowsky and C. Janiak, *Organometallics*, 2018, **37**, 298–308.
57 L. Schmolke, S. Lerch, M. Bülow, M. Siebels, A. Schmitz, J. Thomas, G. Dehm, C. Held, T. Strassner and C. Janiak, *Nanoscale*, 2019, **11**, 4073–4082.
58 K. Schütte, J. Barthel, M. Endres, M. Siebels, B. M. Smarsly, J. Yue and C. Janiak, *ChemistryOpen*, 2017, **6**, 137–148.
59 M. Siebels, C. Schlüsener, J. Thomas, Y.-X. Xiao, X.-Y. Yang and C. Janiak, *J. Mater. Chem. A*, 2019, **7**, 11934–11943.
60 S. Wegner, C. Rutz, K. Schütte, J. Barthel, A. Bushmelev, A. Schmidt, K. Dilchert, R. A. Fischer and C. Janiak, *Chem.–Eur. J.*, 2017, **23**, 6330–6340.
61 C. Vollmer and C. Janiak, *Coord. Chem. Rev.*, 2011, **255**, 2039–2057.
62 S. Watanabe, H. Seguchi, K. Yoshida, K. Kifune, T. Tadaki and H. Shiozaki, *Tetrahedron Lett.*, 2005, **46**, 8827–8829.
63 V. Kelsen, B. Wendt, S. Werkmeister, K. Junge, M. Beller and B. Chaudret, *Chem. Commun.*, 2003, **49**, 3416–3418.
64 C. Amiens, B. Chaudret, D. Ciuculescu-Pradines, V. Collière, K. Fajerwerg, P. Fau, M. Kahn, A. Maisonnat, K. Soulantica and K. Philippot, *New J. Chem.*, 2013, **37**, 3374–3401.
65 J. Krämer, E. Redel, R. Thomann and C. Janiak, *Organometallics*, 2008, **27**, 1976–1978.
66 C. Janiak, in *Ionic Liquids (ILs) in Organometallic Catalysis*, ed. J. Dupont and L. Kollár, Springer-Verlag Berlin Heidelberg, 2015, pp. 38–42.
67 K. Soulantica, A. Maisonnat, M.-C. Fromen, M.-J. Casanove, P. Lecante and B. Chaudret, *Angew. Chem., Int. Ed.*, 2001, **40**, 448–451.
68 Z. Tshemese, M. D. Khan, S. Mlowe and N. Revaprasadu, *Mater. Sci. Eng., B*, 2018, **227**, 116–121.
69 K. Klauke, B. Hahn, K. Schütte, J. Barthel and C. Janiak, *Nano-Struct. Nano-Objects*, 2015, **1**, 24–31.
70 D. König, K. Richter, A. Siegel, A.-V. Mudring and A. Ludwig, *Adv. Funct. Mater.*, 2014, **24**, 2049–2056.
71 T. Löffler, H. Meyer, A. Savan, P. Wilde, A. Garzón Manjón, Y. T. Chen, E. Ventosa, C. Scheu, A. Ludwig and W. Schuhmann, *Adv. Energy Mater.*, 2018, **8**, 1802269.

 This journal is © The Royal Society of Chemistry 2020

Open Access Article. Published on 31 March 2020. Downloaded on 2/6/2026 9:28:58 AM.
This article is licensed under a Creative Commons Attribution-NonCommercial 3.0 Unported Licence.

72 T. Löffler, A. Savan, A. Garzón Manjón, M. Meischein, C. Scheu, A. Ludwig and W. Schuhmann, *ACS Energy Lett.*, 2019, **4**, 1206–1214.
73 T. Löffler, A. Savan, H. Meyer, M. Meischein, V. Strotkötter, A. Ludwig and W. Schuhmann, *Angew. Chem., Int. Ed.*, 2020, **59**, 5844–5850.
74 M. Meischein, A. Garzón-Manjón, T. Frohn, H. Meyer, S. Salomon, C. Scheu and A. Ludwig, *ACS Comb. Sci.*, 2019, **21**, 743–752.
75 G. Beamson and D. Briggs, *J. Chem. Educ.*, 1993, **70**, A25.
76 B. R. Strohmeier, *Surf. Interface Anal.*, 1990, **15**, 51–56.
77 M. C. Biesinger, B. P. Payne, A. P. Grosvenor, L. W. M. Lau, A. R. Gerson and R. S. T. C. Smart, *Appl. Surf. Sci.*, 2011, **257**, 2717–2730.
78 V. Amendola, R. Pilot, M. Frasconi, O. M Maragò and M. A. Iatì, *J. Phys.: Condens. Matter*, 2017, **29**, 203002.
79 V. G. Yarzhemskii, M. A. Kazaryan and E. N. Murav'ev, Electronic structure and optical properties of gold nanoparticles, *Bull. Lebedev Phys. Inst.*, 2012, **39**, 254–256.
80 Y. Li, Y. Liu and J. Yang, *Opt. Laser Technol.*, 2020, **122**, 105875.
81 J. Zhao, A. O. Pinchuk, J. M. McMahon, S. Li, L. K. Ausman, A. L. Atkinson and G. C. Schatz, *Acc. Chem. Res.*, 2008, **41**, 1710–1720.
82 A. Garzón-Manjón, H. Meyer, D. Grochla, T. Löffler, W. Schuhmann, A. Ludwig and C. Scheu, *Nanomaterials*, 2018, **8**, 903–914.